Influence of Wind-Induced Antenna Oscillations on Radar Observations

Pao-Liang Chang, Wei-Ting Fang, Pin-Fang Lin, and Yu-Shuang Tang

Central Weather Bureau

Abstract

As Typhoon Goni (2015) passed over Ishigaki Island, a maximum gust speed of 71 m s^{-1} was observed by a surface weather station. During Typhoon Goni's passage, mountaintop radar recorded antenna elevation angle oscillations, with a maximum amplitude of ~ 0.2° at an elevation angle of 0.2°. This oscillation phenomenon was reflected in the reflectivity and Doppler velocity fields as Typhoon Goni's eyewall encompassed Ishigaki Island.

The main antenna oscillation period was approximately 0.21-0.38 s under an antenna rotational speed of ~4 rpm. The estimated fundamental vibration period of the radar tower is approximately 0.25-0.44 s, which is comparable to the predominant antenna oscillation period and agrees with the expected wind-induced vibrations of buildings. The reflectivity field at the 0.2° elevation angle exhibited a phase shift signature and a negative correlation of -0.5 with the antenna oscillation, associated with the negative vertical gradient of reflectivity.

FFT analysis revealed two antenna oscillation periods on 23 Aug 2015 at 0955-1205 UTC and 1335-1445 UTC. The oscillation phenomenon ceased between these two periods because Typhoon Goni's eye moved over the radar site. The VAD analysis-estimated wind speeds at a range of 1 km for these two antenna oscillation periods exceeded 45 m s^{-1}, with a maximum value of approximately 70 m s^{-1}.

Key word: Typhoon, radar, antenna oscillation. FFT, VAD

1. Introduction

Extremely strong winds frequently damage or destroy electric power supplies, telecommunications equipment, and radar hardware, including radomes and antennas. As an example, the Weather Surveillance Radar, 1988 Doppler (WSR-88D) at Wu-Feng-San operated by the Central Weather Bureau (CWB) of Taiwan was destroyed by Typhoon Herb (1996), which produced maximum sustained surface winds of 65 m s^{-1} (Wu et al. 2002). In 2013, Super Typhoon Haiyan made landfall near Guiuan in the eastern-central Philippines, and the pedestal of the Guiuan radar was sheared off by 1-min sustained winds that possibly reached 91 m s^{-1} (Velden et al. 2017). In 2017, the WSR-88D radar operated by the National Weather Service (NWS) was destroyed by Hurricane Maria's powerful winds, with 1-min maximum sustained wind speed intensities estimated at 70 m s^{-1} as the hurricane moved onshore in southeastern Puerto Rico (Garcia-Rivera 2018).

Even if the radome can resist extremely strong winds, the quality of radar observations will be influenced by wind-induced vibration of the radar tower (e.g., Lagos and Kupeer 2012; Xu et al. 2014). As a result, the quality of radar-derived weather monitoring and forecasting products, such as for severe weather detection (e.g., Johnson, et al. 1998; Stumpf 1998), radar quantitative precipitation estimation (QPE), quantitative precipitation forecast (QPF), and high-resolution radar data assimilation, will potentially be reduced. The natural vibration of a building or tower can be triggered by strong wind or earthquakes; the more uniform and symmetrical the form of the structure is, the more likely the structure will oscillate under windy conditions (e.g., Lagos and Kupeer 2012; Xu et al. 2014). Generally, the natural vibration period is proportional to the building height. Once buildings or towers vibrate, objects mounted on them (such as radomes) will oscillate in tandem.

The rapid intensification of Typhoon Goni (2015) was observed by the Ishigaki (ISHI) C-band Doppler radar on Ishigaki Island operated by the Japan Meteorological Agency (JMA) (Shimada et al. 2018). As Typhoon Goni passed near Ishigaki Island between 1000 Coordinated Universal Time (UTC) and 1400 UTC on 23 Aug 2015, the eyewall and eye moved over the radar site. At this time, the maximum wind speed estimated from the Doppler velocity at a radius of 1 km at a 1.1° elevation angle exceeded 70 m s^{-1}, which resulted in antenna oscillations that impacted the reflectivity and Doppler velocity fields, with an unusual oscillation pattern. In this study, the wind speed thresholds for antenna oscillations and the influences of these

oscillations on radar observations are investigated and discussed.

2. Data and methodology

The C-band Doppler ISHI radar on Ishigaki Island operated by the JMA is used in this study. Table 1 shows the radar parameters and scanning strategy for the ISHI radar. Two surveillance and Doppler modes with a total of 26 sweeps for 13 elevation angles are alternately operated and updated every 10 min for the ISHI radar. To integrate more volume scans, radar data from the second Doppler (D_2) and surveillance (S_2) modes are chosen for wind and reflectivity analyses, respectively. For convenience in these analyses, the volume scan time is set to 5 min after the onset of the first Doppler mode (D_1). Additionally, the ISHI radar is operated in dual-pulse repetition frequency (PRF) mode to extend the maximum unambiguous velocity. Although the Nyquist velocity can be extended to 52.71 m s^{-1}, the Doppler velocity field would still encounter the folding problem when the wind speeds exceed the Nyquist velocity in the inner core region of Typhoon Goni. Therefore, the vortex-based Doppler velocity dealiasing (VDVD) algorithm (Chang et al. 2019) is applied to recover the aliased Doppler velocities.

Based on the recorded radar data from each beam, the angular wavenumbers (hereafter called wavenumbers) of the antenna oscillations centered on the radar site with different ranges and elevations are analyzed using the FFT algorithm. Each ISHI radar plan position indicator (PPI) scan includes 512 azimuths at a resolution of approximately 0.7°. Therefore, one-dimensional spatial FFT analysis is applied to decompose the radar reflectivity and Doppler velocity data into a series of wavenumbers from 0 to 200 at a constant radius and elevation. Based on the rotational speed of the radar antenna, the predominant oscillation periods (frequencies) can be determined by selecting the wavenumbers of crucial components.

3. Results

a. Oscillation features

The radar data from Typhoon Goni between 0705 UTC and 1705 UTC on 23 Aug 2015 are selected to investigate the influence of extremely strong winds on radar observations. Figure 1 shows a reflectivity example from the ISHI radar at 1155 UTC on 23 Aug 2015. At the lowest elevation angle of -0.4°, the eyewall structure is well organized with a radius of approximately 25 km, while the eastern part of the eyewall covers the radar site. The regular radial pattern with alternating strong and weak features is very pronounced, although this periodic pattern nearly obscures the eyewall, low-reflectivity and spiral rainband regions. In addition, a band with enhanced reflectivities is found southeast of the radar site, which possibly results from sea clutter signals. At -0.1°, the regular radial pattern is still pronounced, whereas the intensity of the enhanced band in the southeastern quadrant is relatively weak, but the radial oscillation pattern is still significantly similar to that at -0.4°. At an elevation angle of 0.2°, the oscillation phenomenon is still obvious but generally weak and occurs mainly along the low-reflectivity region. This obvious oscillation phenomenon is not clearly observed at 2.7°, possibly because the vertical reflectivity gradients are generally weak compared with the observations at lower elevation angles. Moreover, the oscillation signals occur in limited areas around the outer rainband regions. Although the oscillation signals are more significant at an elevation angle of -0.1° than at any other elevation angle, the temporal evolution of available reflectivity (Fig. 2) and Doppler velocity (Fig. 3) observations at an elevation angle of 0.2° is documented every 30 min from 1125 UTC to 1355 UTC during Typhoon Goni's passage near Ishigaki Island.

The regular radial pattern in the reflectivity already exists in the low-reflectivity region at 1125 UTC (Fig. 2a), at which time the oscillation phenomenon is comparable to that at 1155 UTC (Fig. 2b). Between 1225 and 1325 UTC (Fig. 2c to 2e), the oscillation phenomenon disappears as the outer boundary of the eye region passes over the radar site. At 1355 UTC (Fig. 2f), the oscillation phenomenon reappears, although the strength of the signal clearly decreases. After 1425 UTC (not shown), the oscillation phenomenon disappears as Typhoon Goni continuously moves northwestward away from the radar site..

For the corresponding Doppler velocity field, the eyewall region is obviously characterized by an approximately symmetric dipole signature with a maximum magnitude exceeding 60 m s^{-1} at 1125 UTC at an elevation angle of 0.2° (Fig. 3a). Outside the eyewall region, oscillation phenomena can be observed in part of the low-reflectivity and spiral rainband regions located in the northern and eastern quadrants of the typhoon. A similar but slightly weaker oscillation signature can also be found in the spiral rainband region in the southern quadrant of the typhoon. As the outer boundary of the eye region passes over the radar site (Figs. 3c to 3e) from 1225 UTC to 1325 UTC, the maximum/minimum Doppler velocity observations are underestimated due to geometric distortion (Wood and Brown 1992), and the oscillation phenomenon dramatically disappears over time (Figs. 3c to 3e), similar to that in the reflectivity field (Figs. 2c to 2e). At 1355 UTC (Fig. 3f), the maximum/minimum inbound/outbound Doppler velocities are comparable to those from 1125 UTC to 1155 UTC because the eyewall region gradually moves away from the radar site and the abovementioned geometric distortion disappears. Compared to the oscillation phenomenon in the reflectivity field shown in Fig. 2f, the signature in the Doppler velocity is less significant. Because Doppler radars measure only the velocity of precipitation particles along the viewing direction, the amplitudes of the oscillation signals in the Doppler velocity field are not comparable among different azimuths even though the winds are

horizontally homogenous; the vertical gradient of the Doppler velocity field enhances the variation in the oscillation signals, as shown in the reflectivity field.

b. Oscillation analyses

Antenna oscillations substantially affect radar observations, as shown in Figs. 1 through 3. Figure 8a shows the azimuthal distribution of reflectivity at an elevation angle of 0.2° and a range of 50 km at 1155 UTC on 23 Aug 2015. The reflectivity intensities range from 8 to 44 dBZ for all azimuths and present high-frequency oscillations with a maximum amplitude of 16 dB at azimuths of approximately 330-360°. Fig. 4s with wavenumbers ranging from 0 to 200 fits the reflectivity data well. Similar to the reflectivity oscillation results, the hardware-recorded elevation angle as a function of azimuth shows significant high-frequency oscillations, with a maximum amplitude of ~0.2° at an azimuth of approximately 60° (Fig. 4b). The curve composed of the wavenumbers from the FFT analysis also well fit the hardware-recorded elevation angle data.

Because the antenna and reflectivity oscillations are significant and primarily contributed by wavenumbers from 40 to 70 shown in Fig. 4a, wavenumbers in these ranges are extracted to highlight the phase relationship between the antenna and reflectivity oscillation signals although the other wavenumbers could partially contribute to the oscillation signals. A phase shift signature (Fig. 5) and a negative correlation (correlation coefficient of -0.5) are found between the antenna and reflectivity oscillation signals decomposed from wavenumbers 40 to 70. This finding indicates that oscillating reflectivity values will decrease (increase) as the antenna elevation angle increases (decreases) during an antenna oscillation period . The reflectivity field exhibits an oscillation approximately 180° out of phase with the antenna oscillation because the radar beams point toward the ocean and detect sea clutter or the strong reflectivity gradient when the amplitude of the elevation angle is negative, and vice versa.

For the Doppler velocity field at 0.2° in the range of 50 km (Fig. 6), oscillation signals are still present, but the amplitudes are not comparable to those in the reflectivity field. As mentioned above, the amplitudes of the oscillation signals in the Doppler velocity field are not comparable among different azimuths, and the strong vertical gradient of Doppler velocities in the eyewall region enhances the variation in oscillation signals, as observed at azimuths of 0°-45°, whereas sea clutter contributes to the significant signals detected at azimuths of 300°-360°.

From the analyses of the elevation angle amplitudes for different wavenumbers and 13 preset elevation angles from -0.4° to 25.0° (Fig. 7a), amplitudes greater than 0.02° occur at wavenumbers of approximately 45 to 70 for all elevation angles. Based on the given antenna rotational speed of 4 rpm for the ISHI radar, the corresponding frequencies (periods) range from 2.67 s^{-1} (0.38 s) to 4.67 s^{-1} (0.21 s). In addition, antenna oscillations influence the data at all elevation angles, with a maximum elevation angle amplitude greater than 0.08° at wavenumber 56 at an elevation angle of 1.1°. Reflectivity amplitudes for different wavenumbers and 13 preset elevation angles from -0.4° to 25.0° are shown in Fig. 7b. FFT analyses are not performed for elevation angles of 17.2° and 25.0° because the available quantity of data is less than half (256) of the full radar range at 50 km. The reflectivity FFT analysis demonstrates that relatively large amplitudes are confined to elevation angles < 0.6° and that the maximum reflectivity amplitude larger than 1 dB occurs at -0.1° for wavenumbers between approximately 45 and 60. Notably, the maximum amplitude with a value greater than 2 dB is found at the elevation angle of -0.1° rather than at the lowest elevation angle of -0.4°, indicating that the oscillation signals at -0.4° are seriously contaminated by sea clutter signals, because of the decreasing vertical reflectivity gradient at this elevation angle. The oscillation signals at higher elevations are much weaker than those at lower elevations, as documented in section 3a.

Regarding the Doppler velocity amplitudes for different wavenumbers over 9 preset elevation angles from 0.2° to 25.0° (Fig. 7c), relatively weak signals are discovered compared with those in the reflectivity field. The most significant signals occur at the lowest elevation angle of 0.2°, with a maximum value greater than 1.5 m s^{-1} approximately between wavenumbers 48 and 55. Furthermore, the oscillation signal amplitudes larger than 0.5 m s^{-1} are found over a wide wavenumber range, indicating that more noise is triggered in the Doppler velocity fields. This finding indicates that oscillation signals are enhanced by the vertical gradient of the Doppler velocity and the contamination by sea clutter signals under the unequal amplitude responses at certain azimuths to antenna oscillations, as mentioned in section 3a.

c. Velocity-azimuth display (VAD) analysis

Because there are no wind observations at the ISHI radar site, which is located near the top of Mt. Omoto-dake (525.5 m above sea level), VAD analyses (Lhermitte and Atlas 1961; Browning and Wexler 1968) are conducted to estimate the wind speeds during Typhoon Goni's passage. However, the assumption of linearity utilized in the VAD algorithm tends to break down when intense cyclonic storms, such as tropical cyclones, are considered (Donaldson and Harris 1989). Furthermore, to avoid the influences of Doppler velocity fluctuations due to ground clutter and antenna oscillations at the lowest elevation angle of 0.2°, Doppler velocity data for an elevation angle of 1.1° at a radial distance of 1 km are chosen for the VAD analysis. The temporal period for VAD winds is less than 18 s.

Figure 8 shows a Hovmöller diagram of the elevation angle amplitudes for wavenumbers 0 to 100 between 0705 UTC and 1705 UTC on 23 Aug 2015 at a

preset elevation angle of -0.1°. The wind speeds derived from the VAD analysis in the same analyzed period are overlaid. Elevation angle oscillation amplitudes exceeding 0.02° between wavenumbers 45 and 70 are found between 0955 UTC and 1205 UTC and between 1335 UTC and 1445 UTC. The most pronounced elevation angle oscillation amplitudes greater than 0.03° in the first oscillation period occur at 1155 UTC for wavenumbers between 45 and 70. In the second oscillation period, the most pronounced amplitudes greater than 0.03° occur at 1405 UTC for wavenumbers between 45 and 60. These high amplitudes in the wavenumber 40-70 band are not found between these two oscillation periods.

Based on a comparison with the VAD-retrieved winds, the amplitudes in the wavenumber 40-70 band increase when the wind speeds are greater than 45 m s^{-1} and significantly decrease when the wind speeds are equal to and lower than 45 m s^{-1}, especially for the period of quiescence between the two periods of pronounced amplitudes. These results imply that wind-induced radar tower vibrations cause antenna oscillations (e.g., Tuan and Shang 2014) and influence the quality of both reflectivity and Doppler velocity fields.

4. Conclusions

This study investigates the antenna oscillation phenomena caused by extremely strong wind speeds produced within Typhoon Goni's eyewall that encompassed Ishigaki Island. The ISHI C-band Doppler radar operated by the JMA is used to investigate the influences of extremely strong wind speeds on reflectivity and Doppler velocity fields. The radar hardware recorded antenna elevation angle oscillations with a maximum amplitude of ~ 0.2° at a 0.2° elevation angle at 1155 UTC on 23 Aug 2015. The corresponding reflectivity intensities present high-frequency oscillations with a maximum amplitude of 16 dB. Via FFT analysis, the predominant oscillation period is calculated as approximately 0.25-0.33 s. Additionally, two antenna oscillation periods are found; between these two oscillation periods, the oscillation phenomenon disappeared with decreasing wind speed when Typhoon Goni's eye moved over the radar site. Moreover, maximum amplitudes of elevation angle oscillations greater than approximately 0.02° for wavenumbers 45-70 are found between 0955 UTC and 1205 UTC and between 1335 UTC and 1445 UTC during Typhoon Goni's passage. The wind speeds estimated from VAD analysis at a range of 1 km for the two antenna oscillation periods are greater than 45 m s^{-1}, with a maximum value of approximately 70 m s^{-1}. The surface station on Ishigaki Island also observed a maximum gust wind speed of 71 m s^{-1}. Although the wind speed estimations and observations differ with regard to both altitude and instrumentation, the temporal evolutions of the wind speeds are similar except for the period when Typhoon Goni's eye moved over the radar site. The large differences during the passage of Typhoon Goni's eye could have been contributed by differences in the horizontal and vertical wind structures of the typhoon circulation.

Regarding the reflectivity oscillation signal, the antenna oscillations are approximately 180° out of phase and generally consistent with the vertical gradient of reflectivity. The Doppler velocity field is also influenced by the antenna oscillations, although the oscillation signals are relatively less pronounced since the oscillation signals are also a function of the wind direction and radar azimuth in addition to the vertical gradient. To further investigate this phenomenon, the influences of antenna oscillations on radar reflectivity are simulated. Beam patterns with different amplitudes can also be adequately simulated, implying that the vertical gradient dominates the strength of the oscillation phenomenon, especially in regions with sea clutter.

To reduce the influences of antenna oscillations on radar observations, a bandpass filter QC procedure is applied by filtering out the predominant wavenumbers (between 40 and 70) on individual rings for both the reflectivity field and the Doppler velocity field (Chang et al. 2020). As a consequence, oscillation signals can be significantly mitigated, although weak oscillation signals remain near the low-reflectivity and spiral rainband regions. The QC issue in the Doppler velocity field is more complicated than that in the reflectivity field, and thus, a two-step procedure is conducted. Most beam patterns in the Doppler velocity field can be properly eliminated compared with the data before the implementation of the QC procedure.

The estimated fundamental vibration periods are comparable to the predominant periods analyzed based on reflectivity observations, with values of 0.33 s and 0.5 s. The results are essentially consistent with the expected wind-induced vibrations of buildings, which could be adequately mitigated if extremely strong wind conditions are considered in the design of radar towers. Detailed oscillation simulations are suggested for future research, such as wind tunnel tests and associated analyses, to provide solutions for mitigating the vibrational effects of radar towers under extremely strong wind conditions.

References

Browning, K. A., and R. Wexler, 1968: The determination of kinematic properties of a wind field using Doppler radar. *J. Appl. Meteor.*, **7,** 105–113.

Chang, P. -L., W. -T. Fang, P. -F. Lin, and M. -J. Yang, 2019: A vortex-based Doppler velocity dealiasing algorithm for tropical cyclones. *J. Atmos. Oceanic Technol.*, **36,** 1521-1545.

——, ——, ——, and Y. -S. Tang, 2020: Influence of Wind-Induced Antenna Oscillations on Radar Observations and Its Mitigation. *Wea. Forecasting*, doi: https://doi.org/10.1175/WAF-D-20-0064.1.

Garcia-Rivera, M. Jose, 2018: Hurricane Maria in Puerto Rico: Structure and intensity evolution prior to

landfall. *33rd Conference on Hurricanes and Tropical Meteorology*, American Meteorological Society (AMS), Ponte Vedra, FL, US.

Lagos, R., and M. Kupeer, 2012: Performance of high-rise buildings under the February 27th 2010 Chilean earthquake. *Proceedings of the International Symposium on Engineering Lessons Learned from the 2011 Great East Japan Earthquake*. Tokyo, Japan, pp. 1754–1765.

Lhermitte, R. M., and D. Atlas, 1961: Precipitation motion by pulse Doppler. *Proc. Ninth Weather Radar Conf.*, Kansas City, MO, Amer. Meteor. Soc., 218-223.

Shimada, U., M. Sawada, and H. Yamada, 2018: Doppler radar analysis of the rapid intensification of Typhoon Goni (2015) after eyewall replacement. *J. Atmos. Sci.,* **75,** 143–162.

Velden, C., T. Olander, D. Herndon, and J. P. Kossin, 2017: Reprocessing the most intense historical tropical cyclones in the satellite era using the advanced Dvorak technique. *Mon. Wea. Rev.*, **145,** 971–983.

Wood, V. T., and R. A. Brown, 1992: Effects of radar proximity on single-Doppler velocity signatures of axisymmetric rotation and divergence. *Mon. Wea. Rev.,* **120,** 2798–2807.

Wu, C. -C., T. -H. Yen, Y. -H. Kuo, and W. Wang, 2002: Rainfall simulation associated with Typhoon Herb (1996) near Taiwan. Part I: The topographic effect. *Wea. Forecasting*, **17,** 1001–1015.

Xu, P., C. Xiao, and J. Li, 2014: Research on relationship between natural vibration periods and structural heights for high-rise buildings and its reference range in China. *International Journal of High-Rise Buildings*, 3(1), 49–64.

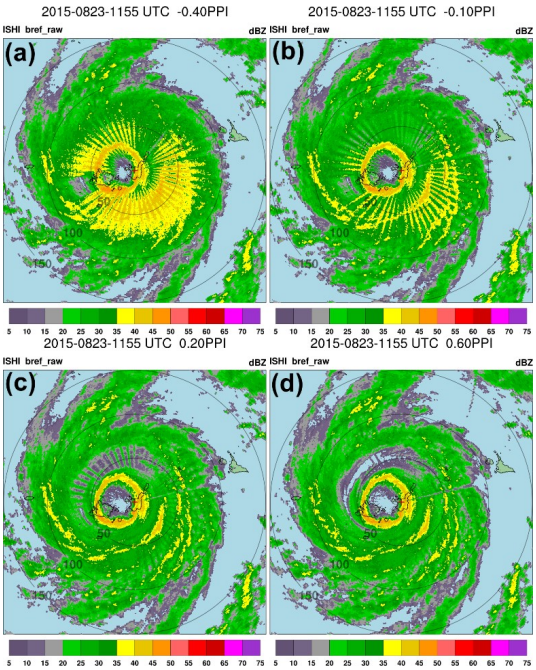

Figure 1. Reflectivity fields at elevation angles of (a) -0.4°, (b) -0.1°, (c) 0.2°, and (d) 0.6° from the ISHI radar at 1155 UTC on 23 Aug 2015. The radar position is indicated by a pink cross.

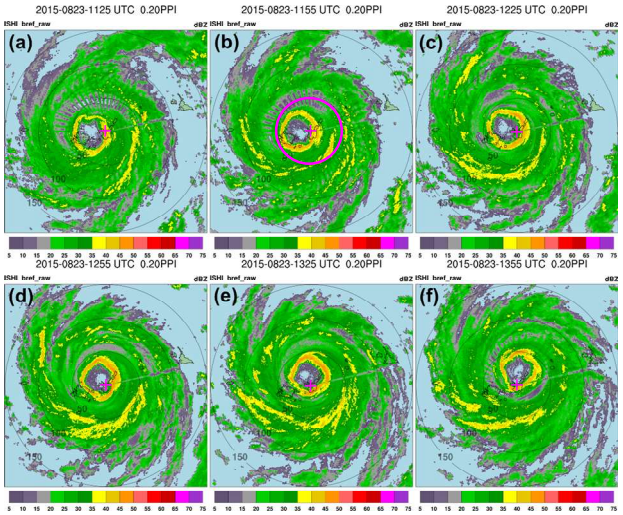

Figure 2. Temporal evolution of the reflectivity fields from the ISHI radar every 30 min at an elevation angle of 0.2° from 1125 UTC to 1355 UTC on 23 Aug 2015. The radar position is indicated by a pink cross, and the data in the range of 50 km from the radar site shown in (b) with a pink ring are used for the oscillation analyses in Fig. 4 and Fig. 7.

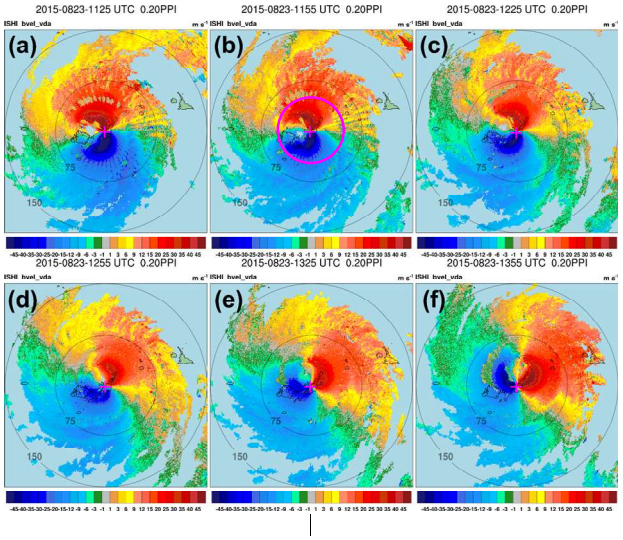

Figure 3. Same as Fig. 2 except for the Doppler velocity field, and the data in the range of 50 km from the radar site shown in (b) with a pink ring are used for the oscillation analyses in Fig. 4 and Fig. 7.

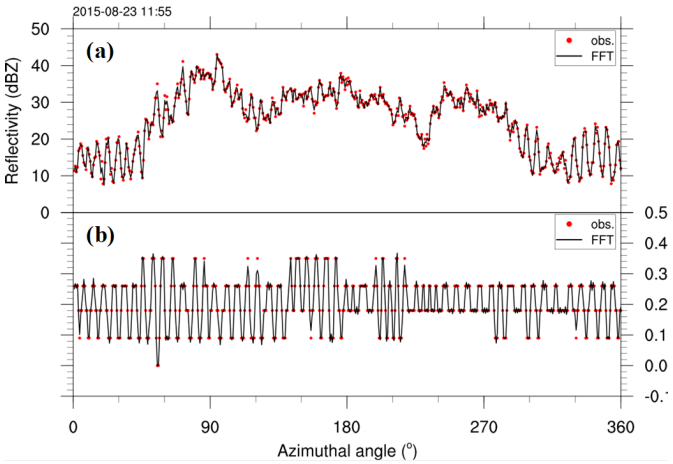

Figure 4. Azimuthal distributions of the (a) reflectivity and (b) elevation angle at an elevation angle of 0.2° in the range of 50 km from the radar site (as shown in Fig. 3b) at 1155 UTC on 23 Aug 2015. The red dots indicate the observed reflectivities and elevation angles, and the associated black curves are generated based on the wavenumbers calculated from the FFT analysis.

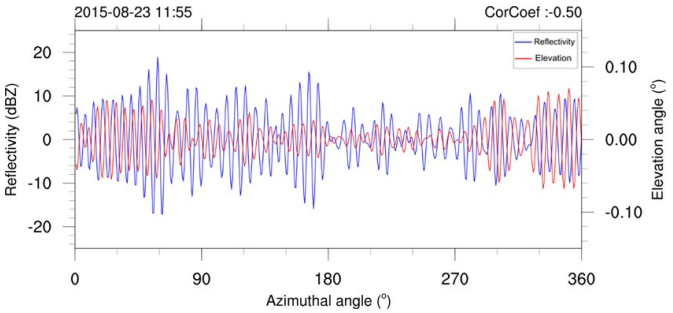

Figure 5. Same as Fig. 4 except for the azimuthal distributions of the reflectivity (blue curve) and elevation angle amplitudes (red curve) at an elevation angle of 0.2° generated based on wavenumbers from 40 to 70.

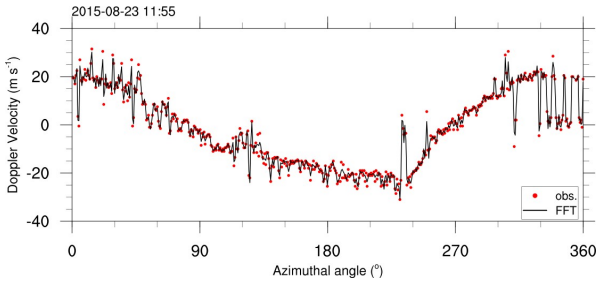

Figure 6. Same as in Fig. 4 except for the azimuthal distribution of Doppler velocities at an elevation angle of 0.2°.

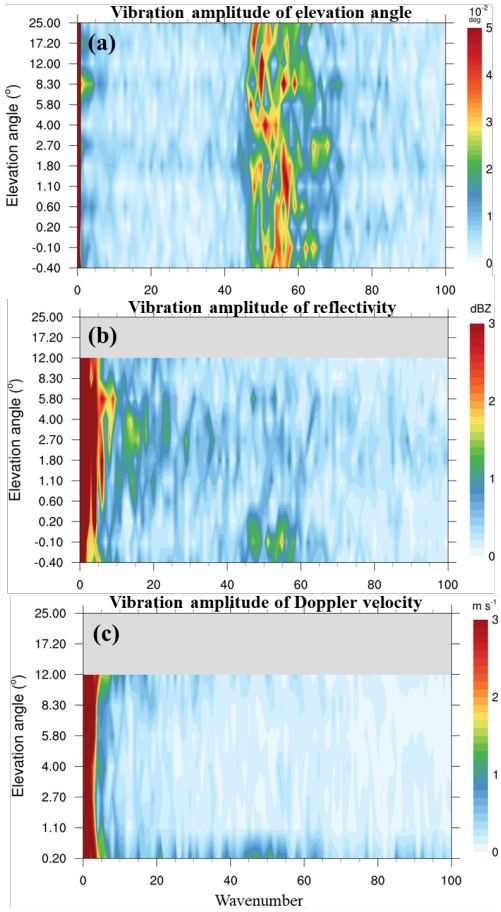

Figure 7. (a) Elevation angle, (b) reflectivity, and (c) Doppler velocity amplitudes as a function of wavenumber for 13 preset elevation angles from -0.4° to 25.0° at 1155 UTC on 23 Aug 2015. The elevation angle and reflectivity volume data are combined from surveillance and Doppler modes. The Doppler velocity volume data are only from the Doppler mode.

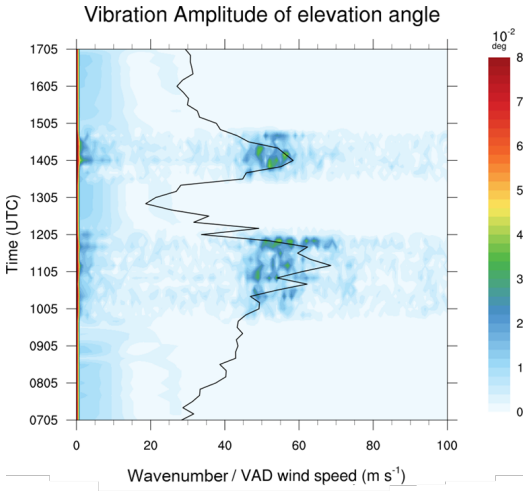

Figure 8. Temporal composite of the elevation angle amplitudes at a preset elevation angle of -0.1° as a function of wavenumber derived from the FFT analysis between 0705 UTC and 1705 UTC on 23 Aug 2015. The solid line indicates the VAD wind speeds.